HHS Public Access

Author manuscript

Oncogene. Author manuscript; available in PMC 2021 July 21.

Published in final edited form as:

Oncogene. 2021 March ; 40(9): 1644–1658. doi:10.1038/s41388-020-01637-w.

Pharmacological and Genetic Perturbation Establish SIRT5 as a Promising Target in Breast Cancer

Yashira L. Negrón Abril[1,*], **Irma R. Fernandez**[1,2,*], **Jun Young Hong**[2], **Ying-Ling Chiang**[2], **Dennis A. Kutateladze**[2], **Qingjie Zhao**[2], **Min Yang**[2], **Jing Hu**[2], **Sushabhan Sadhukhan**[2], **Bo Li**[2,4], **Bin He**[2,6], **Brenna Remick**[1], **Jessica Jingyi Bai**[2], **James Mullmann**[1,4], **Fangyu Wang**[4], **Viviana Maymi**[1], **Ravi Dhawan**[1], **Johan Auwerx**[3], **Teresa Southard**[1], **Richard A. Cerione**[2,4], **Hening Lin**[2,5,#], **Robert S. Weiss**[1,#]

[1]Department of Biomedical Sciences, Cornell University, Ithaca, NY 14853, USA [2]Department of Chemistry and Chemical Biology, Cornell University, NY 14853, USA [3]Laboratory for Integrative Systems Physiology, Institute of Bioengineering, Ecole Polytechnique Fédérale de Lausanne (EPFL), CH-1015 Lausanne, Switzerland [4]Department of Molecular Medicine, Cornell University, NY 14853, USA [5]Howard Hughes Medical Institute; Department of Chemistry and Chemical Biology, Cornell University, NY 14853, USA [6]Current Address: School of Pharmacy, Guizhou Medical University, Guiyang 550004, China

Abstract

SIRT5 is a member of the sirtuin family of NAD^+-dependent protein lysine deacylases implicated in a variety of physiological processes. SIRT5 removes negatively charged malonyl, succinyl, and glutaryl groups from lysine residues and thereby regulates multiple enzymes involved in cellular metabolism and other biological processes. SIRT5 is overexpressed in human breast cancers and other malignancies, but little is known about the therapeutic potential of SIRT5 inhibition for treating cancer. Here we report that genetic *SIRT5* disruption in breast cancer cell lines and mouse models caused increased succinylation of IDH2 and other metabolic enzymes, increased oxidative stress, and impaired transformation and tumorigenesis. We therefore developed potent, selective, and cell permeable small molecule SIRT5 inhibitors. SIRT5 inhibition suppressed the transformed properties of cultured breast cancer cells and significantly reduced mammary tumor growth *in vivo*, in both genetically engineered and xenotransplant mouse models. Considering that *Sirt5*

[#]Co-corresponding authors: Hening Lin < hl379@cornell.edu > and Robert S. Weiss < rsw26@cornell.edu>.
[*]These authors contributed equally to this work;

AUTHOR CONTRIBUTIONS

YLNA, IRF, JYH, RC, HL, RSW conceptualization; YLNA, IRF, JYH, formal analysis; YLNA, IRF, JYH, YLC, DAK, QZ, MY, JH, SS, BL, BH, BR, JJB, RD, JM, FW, VM, TS investigation; YLNA, IRF, JYH, YLC, DAK, QZ, MY, JH, SS, BL, BH, JJB methodology; YLNA, IRF, JYH writing-original draft; YLNA, IRF, JYH, HL, RSW writing-review and editing; JA, RC, HL, RSW resources; RC, HL, RSW funding acquisition; HL, RSW supervision; HL, RSW project administration.

COMPETING INTERESTS STATEMENT

Cornell University has patents on the SIRT5 inhibitors described in the manuscript. The authors have no additional competing interests to declare.

SUPPLEMENTARY INFORMATION

The following is provided as supplementary information: Supplementary Figures S1-10, Supplementary Tables S1-3, and supplementary materials and methods, including the synthesis of all SIRT5 inhibitors.

knockout mice are generally normal, with only mild phenotypes observed, these data establish SIRT5 as a promising target for treating breast cancer. The new SIRT5 inhibitors provide useful probes for future investigations of SIRT5 and an avenue for targeting SIRT5 as a therapeutic strategy.

Keywords

Breast Cancer; Deacylase; SIRT5; Sirtuin; Succinylation

INTRODUCTION

Breast cancer is the most common malignancy in women. Despite advances in early detection and treatment, acquired resistance to chemotherapy and disease recurrence remain a challenge, making breast cancer one of the leading causes of cancer death worldwide [1]. As with other cancers, breast cancers rewire their metabolism to sustain their biosynthetic and bioenergetic needs. Even in the presence of oxygen, cancer cells primarily utilize glucose to produce lactate rather than metabolizing it in the oxidative phosphorylation pathway (the “Warburg effect”) [2]. In addition to altered glucose metabolism, cancer cells increase fatty acid synthesis and glutamine metabolism to fuel their enhanced proliferation. These metabolic changes have been recognized as hallmarks of cancer and are associated with therapy resistance. Thus, much attention has been given to therapies that target cancer metabolism.

Post-translational modifications (PTMs), such as acetylation, succinylation, malonylation and glutarylation, play crucial roles in cancer progression and drug resistance by regulating cell metabolism and signaling pathways [3, 4]. Therefore, targeting enzymes that regulate specific PTMs has therapeutic potential. Protein acetylation, succinylation, malonylation and glutarylation are regulated by sirtuins, a family of nicotinamide adenine dinucleotide (NAD^+)-dependent protein deacylases [5–7]. Among the seven mammalian sirtuins, SIRT5 localizes primarily to mitochondria and catalyzes NAD^+-dependent demalonylation, desuccinylation, and deglutarylation of metabolic enzymes involved in glycolysis, glutamine metabolism, fatty acid oxidation and the pentose phosphate pathway [8–12]. Sirtuins have been implicated in regulating cancer cell metabolism [13–15], and recent findings indicate that SIRT5 is overexpressed in multiple cancer types and can be associated with poor patient outcomes [16–19]. Furthermore, SIRT5 promotes cancer cell proliferation by targeting multiple metabolic enzymes, including GLS, SHMT2, and PKM2 [20–22]. Recent studies have also implicated SIRT5 in protecting cells from reactive oxygen species (ROS) by activating SOD1, IDH2 and G6PD [23, 24].

Despite reports that SIRT5 may be important for cancer cells, it remains unknown whether pharmacological SIRT5 inhibition is a viable approach for treating human cancers. To date, no small molecule SIRT5 inhibitors have been tested in cancer models. This is mainly due to the lack of potent, selective, and cell permeable SIRT5 inhibitors. Several laboratories have reported SIRT5 inhibitors, but most are not cell permeable or were not tested in cancer cell lines or animal models [25–30]. Only one SIRT5 inhibitor, MC3482, has been reported to

inhibit SIRT5 in cells and affect glutamine metabolism, but it is of low potency (< 50% SIRT5 inhibition *in vitro* at 100 μM) and its anticancer activity was not investigated [14].

Here, we developed potent and cell permeable SIRT5-specific small molecule inhibitors to test the therapeutic potential of targeting SIRT5 for treating breast cancer. We also employed genetic approaches to demonstrate that SIRT5 loss suppressed malignant transformation in cultured cells and reduced mammary tumor progression and delayed lung metastasis in the MMTV-PyMT mouse model. Moreover, SIRT5 inhibitor treatment reduced tumor burden in MMTV-PyMT mice, as well as in a triple-negative breast cancer xenograft model. The small molecule inhibitors described here represent useful probes for future SIRT5 investigations and establish for the first time that pharmacological SIRT5 inhibition has anticancer effects *in vivo*.

RESULTS

SIRT5 is overexpressed in human breast cancers.

To evaluate SIRT5 alterations in breast cancer, we interrogated The Cancer Genome Atlas (TCGA) and Molecular Taxonomy of Breast Cancer International Consortium (METABRIC) datasets using cBioPortal [31]. *SIRT5* showed gene amplification or gain in 26.1% (213/817) of invasive breast carcinomas (Figure 1A). *SIRT5* amplification and gain correlated with increased *SIRT5* mRNA expression, and *SIRT5* overexpression was significantly higher in basal-like breast cancer relative to other subtypes (Figure 1B, C). Further stratification based on expression of estrogen and progesterone receptors (ER/PR) and human epidermal growth factor receptor 2 (HER2) showed that *SIRT5* is overexpressed in ER-, PR-, and HER2-negative breast cancer when compared to other subtypes (Supplementary Figure S1A). *TP53* and *MYC* amplification are common in breast invasive carcinomas [32], and analysis of the TCGA data revealed that *SIRT5* copy number amplification and gain was significantly enriched with these recurrently altered genes (Figure 1D and Supplementary Figure S1B, C). *SIRT5* amplification/gain was not correlated with clinical outcome across all TCGA samples, but was associated with significantly poorer overall survival of patients with mixed ductal/lobular breast cancer (Figure 1E and Supplementary Figure S1D, E). Together these data highlight the importance of *SIRT5* overexpression in breast cancer.

SIRT5 deficiency suppresses the proliferation and anchorage-independent growth of human breast cancer cells.

To examine the importance of SIRT5 for malignant transformation, we knocked down *SIRT5* in SKBR3 human breast cancer cells, as well as CRL-5800 human lung cancer cells for comparison, and assessed anchorage-independent growth. *SIRT5* knockdown with two different siRNAs markedly reduced anchorage-independent growth in both cell lines (Figure 2A, B). We further investigated the requirement for SIRT5 in a classic cell transformation model by generating $Sirt5^{+/+}$ and $Sirt5^{-/-}$ mouse embryonic fibroblasts (MEFs) expressing a conditional oncogenic *Kras* allele, *LSL-*$Kras^{G12D}$ [33] (Supplementary Figure S2A-D). $Kras^{G12D}$ stimulated the proliferation of both $Sirt5^{+/+}$ and $Sirt5^{-/-}$ MEFs to a similar extent in 2D culture. However, $Kras^{G12D}$-expressing $Sirt5^{-/-}$ MEFs demonstrated significantly

reduced anchorage-independent growth as compared to *Kras*^{G12D}-expressing *Sirt5*$^{+/+}$ controls, findings that were confirmed in an independent set of MEFs.

We next used CRISPR/Cas9 to disrupt *SIRT5* in MDA-MB-231 triple negative breast cancer cells (Figure 2C) as well as HCT116 colorectal cancer cells (Supplementary Figure S2E). Partial loss of *SIRT5* expression was achieved in two independent clones of MDA-MB-231 cells, while complete knockout was achieved in HCT116 cells. SIRT5 loss hampered proliferation in MDA-MB-231 cells but had minimal effect on HCT116 cells in 2D culture. However, SIRT5 loss inhibited the anchorage-independent growth of both MDA-MB-231 and HCT116 cells (Figure 2D-F and Supplementary Figure S2F-H). Given the striking growth defects in detached conditions following *SIRT5* loss, we also tested the invasive capacity of *SIRT5*-targeted cells *in vitro* using Boyden chambers. Compared to *SIRT5* WT controls, *SIRT5*-deficient MDA-MB-231 cells showed significantly reduced cell migration (Figure 2G, H). Expression of other Sirtuins was not significantly altered following *SIRT5* disruption (Supplementary Figure S2I, J), suggesting a direct role for SIRT5 in anchorage-independent growth and migration.

Impaired mammary tumor progression in *Sirt5*-deficient mice.

We next used mouse mammary tumor virus (MMTV)-polyoma middle T antigen (PyMT) transgenic mice, which feature highly penetrant mammary tumors and lung metastasis [34–36] to determine how *Sirt5* deletion affects mammary tumor formation and metastasis. Tumor onset was slightly delayed in *Sirt5*$^{-/-}$ PyMT mice when compared to *Sirt5*$^{+/+}$ PyMT mice (Figure 3A). Mammary glands from *Sirt5*$^{+/+}$ and *Sirt5*$^{-/-}$ PyMT females at 6 weeks of age (Cohort 3) showed multiple small hyperplastic lesions that were not significantly different between *Sirt5*$^{+/+}$ and *Sirt5*$^{-/-}$ PyMT mice (Figure 3B). To further examine the effect of *Sirt5* deficiency on tumorigenesis, *Sirt5*$^{+/+}$ and *Sirt5*$^{-/-}$ PyMT females were aged until humane endpoints (Cohort 1, tumor size endpoint). *Sirt5* loss suppressed tumor growth and significantly prolonged survival (p value = 0.0256; median survival: 121 days for *Sirt5*$^{+/+}$ vs. 142 days for *Sirt5*$^{-/-}$) (Figure 3C). We then examined tumor burden in *Sirt5*$^{+/+}$ and *Sirt5*$^{-/-}$ PyMT females 50 days after initial tumor detection (Cohort 2). At this early timepoint, tumor size and wet weight were significantly lower in *Sirt5*$^{-/-}$ PyMT mice (0.60 ± 0.18 g) than *Sirt5*$^{+/+}$ PyMT mice (1.4 ± 0.36 g) (p value = 0.0435) (Figure 3D, E). Taken together, these results demonstrate that SIRT5 promotes mammary tumorigenesis in mice.

Mammary tumors collected based on tumor size endpoint criteria (Cohort 1) did not show significant histological differences. Most tumors showed tumor acini with solid sheets of epithelial cells, characteristic of a late carcinoma stage, as well as some necrotic areas (27.3% for *Sirt5*$^{+/+}$ PyMT and 11.1% for *Sirt5*$^{-/-}$ PyMT). Mammary tumors from mice that were euthanized 50 days after initial tumor detection (Cohort 2) showed minor histopathological differences between the two groups (Figure 3F). When classified into the four identifiable tumor progression stages previously established in MMTV-PyMT mice [36, 37], the largest areas in mammary tumors from *Sirt5*$^{+/+}$ PyMT mice were classified as early carcinoma (48%, 11/23) as compared to adenoma/mammary intraepithelial neoplasia (56%, 15/27) in *Sirt5*$^{-/-}$ PyMT mice. We next examined the effect of *Sirt5* loss on cell proliferation and apoptosis in mammary tumors collected 50 days after initial tumor detection. Despite

smaller tumor size in *Sirt5*$^{-/-}$ PyMT mice, there was no significant difference between tumors from *Sirt5*$^{+/+}$ and *Sirt5*$^{-/-}$ PyMT mice in cell proliferation (Ki-67 p value = 0.6282; BrdU p value = 0.700) or apoptosis as determined by TUNEL staining (p value = 0.9307) and cleaved caspase-3 immunoblotting (Supplementary Figure S3A-E).

The MMTV-PyMT mouse model features rapid and highly penetrant lung metastasis. Analysis of H&E-stained lung sections from *Sirt5*$^{+/+}$ PyMT and *Sirt5*$^{-/-}$ PyMT females collected 50 days after initial tumor detection (Cohort 2) revealed that 40% of *Sirt5*$^{+/+}$ PyMT mice, but no *Sirt5*$^{-/-}$ PyMT mice exhibited lung metastases (Figure 3G, H). However, mice euthanized when tumors reached size endpoints (Cohort 1) did not show differences between genotypes in metastatic burden (Supplementary Figure S3F, G). It should be noted that in this cohort, *Sirt5*$^{-/-}$ PyMT mice had a significantly longer period of time with primary mammary tumors before reaching endpoint than control mice, complicating the direct comparison of metastatic burden between genotypes. Collectively, these data indicate that *Sirt5* loss affects tumor growth and delays but does not abolish mammary tumor metastasis.

SIRT5 loss causes increased protein succinylation and oxidative stress.

Because SIRT5 is the primary mammalian enzyme for lysine desuccinylation, we examined global protein succinylation in mammary tumors from *Sirt5*$^{+/+}$ PyMT and *Sirt5*$^{-/-}$ PyMT mice. Succinylation was prominently increased in *Sirt5*$^{-/-}$ PyMT mammary tumor lysates as compared to those from *Sirt5*$^{+/+}$ PyMT controls (Figure 4A). Treatment of *Sirt5*$^{-/-}$ PyMT mammary tumor lysates with recombinant SIRT5 confirmed that SIRT5 regulated the succinylation of numerous proteins (Figure 4B). To identify SIRT5-regulated proteins, we performed a comparative proteomic analysis of succinylated peptides [38]. LC-MS/MS analysis identified 412 lysine succinylation sites across 146 proteins in mammary tumors from *Sirt5*$^{+/+}$ and *Sirt5*$^{-/-}$ PyMT mice. 285 peptides were only succinylated in *Sirt5*$^{-/-}$ PyMT mammary tumors and 86 were highly abundant in *Sirt5*$^{-/-}$ PyMT as compared to *Sirt5*$^{+/+}$ PyMT tumors (Figure 4C and Supplemental Tables S1, 2). 132 proteins were hypersuccinylated in mammary tumors lacking SIRT5, many of which play important roles in cellular metabolism (Figure 4D and Supplemental Table S3).

The succinylation data led us to hypothesize that SIRT5 might support tumor growth by aiding cancer cell metabolic reprogramming, one key element of which is combatting oxidative stress. SIRT5 has been previously shown to suppress ROS levels by regulating targets such as SOD1, GLS, SHMT2, G6PD, and IDH2 [22–24, 39]. Interestingly, we identified IDH2, an NADPH-generating enzyme, as a SIRT5 substrate in mammary tumors (Figure 4D). SIRT5 is established to desuccinylate and activate IDH2 [24], but the importance of this regulation in cancer is not known. Cell detachment from extracellular matrix (ECM) elevates ROS [40]. Cancer cells, but not normal cells, are able to combat elevated ROS and continue growing when removed from the ECM. Consequently, anchorage-independent growth is dependent on IDH2 [41], similar to what we observed with SIRT5. Therefore, we directly tested whether SIRT5 regulates IDH2 lysine succinylation in breast cancer cells. Consistent with a role for SIRT5 as an IDH2 desuccinylase, *SIRT5* loss increased IDH2 lysine succinylation (Figure 4E), suggesting IDH2 desuccinylation and ROS

detoxification as mechanisms by which SIRT5 supports malignant transformation (Figure 4F).

We next tested the hypothesis that SIRT5 protects breast cancer cells from oxidative stress. Reduced glutathione levels were significantly lower in *Sirt5*$^{-/-}$ PyMT than *Sirt5*$^{+/+}$ PyMT mammary tumors (Figure 4G). MDA-MB-231 clones 1 and 2 also showed a significant reduction in total glutathione levels when compared to parental *SIRT5* WT cells (Figure 4H). Glutathione levels were also significantly reduced upon *SIRT5* loss in HCT116 cells, while the $NADP^+$/NADPH ratio increased (Supplementary Figure S4A, B). We next quantified ROS by staining with the fluorogenic dye DCFDA but did not observe differences between *SIRT5* WT MDA-MB-231 cells and *SIRT5* edited clones (Figure 4I). However, DCFDA can only penetrate the outer mitochondrial membrane [42], and the subcellular localization of SIRT5 suggested that SIRT5 might mitigate mitochondrial ROS in particular. We therefore used MitoSOX to measure mitochondrial superoxide levels. *SIRT5*-targeted MDA-MB-231 clones showed significantly increased mitochondrial superoxide as compared to *SIRT5* WT cells (Figure 4J). Interestingly, we observed significantly increased staining with both DCFDA and MitoSOX in *SIRT5*$^{-/-}$ compared to *SIRT5*$^{+/+}$ HCT116 cells (Supplementary Figure S4C, D). Collectively, these data demonstrate that cancer cells rely on SIRT5 to mount important cellular antioxidant defenses and combat mitochondrial ROS, a mechanism that may contribute to anchorage-independent growth and tumor progression.

Development of cell permeable SIRT5-selective inhibitors.

Given that SIRT5 promotes mammary tumorigenesis, SIRT5 inhibitors may have therapeutic potential for treating breast cancer. Because no potent cell permeable SIRT5 inhibitors had been reported, we set out to develop SIRT5 inhibitors to test this idea. We previously demonstrated that a thiosuccinyllysine peptide, H3K9TSu, inhibits SIRT5 selectively *in vitro* [25]. However, H3K9TSu has poor cell permeability and does not show SIRT5 inhibition in cells. To improve cell permeability, we shortened the peptide to a compound, QZ-3a, with a single thiosuccinyllysine residue. After truncation, SIRT5 inhibition was abolished. However, replacing thiosuccinyl with thioglutaryl led to QZ-3b, which showed modest SIRT5 inhibition with an IC_{50} of 43 μM. To simplify the synthesis, we replaced the thioamide with thiourea. Interestingly, the thiourea compound, QZ-I5, had much better SIRT5 inhibition with an IC_{50} of 5.6 μM. Adding a hydroxyl group on the C-terminal benzene ring of QZ-I5 led to JH-I5–2. It has been reported that this additional hydroxyl group provides a hydrogen bond for tighter binding with the sirtuin peptide backbone [43, 44]. Satisfyingly, JH-I5–2 showed stronger SIRT5 inhibition with an IC_{50} of 2.1 μM (Figure 5A).

To increase the potency of SIRT5 inhibition, we replaced the carboxybenzyl group (Cbz) of JH-I5–2 and added an amino acid, leading to four new compounds, YC6–60, YC6–62, DK-106, and DK1–04 (Figure 5B). These dipeptide-based SIRT5 inhibitors showed comparable or lower SIRT5 IC_{50} values than the single lysine-based SIRT5 inhibitors. Among them, DK1–04 portrayed the strongest SIRT5 inhibition with an IC_{50} of 0.34 μM, which was the lowest among the SIRT5 inhibitors tested (Figure 5B). JH-I5–2 and DK1–04, the most potent single lysine-based and dipeptide-based inhibitors, respectively, showed no

inhibition of SIRT1–3 and 6 deacylation activity at 83.3 μM. Next, we explored the inhibitory mechanism by capturing stalled covalent intermediates of DK1–04 and NAD^+. Previously, the thioacetyl peptides or inhibitors were found to form covalent 1'-S-alkylimidate intermediates to inhibit sirtuins [43–46], and we predicted that our SIRT5 inhibitors would form similar stalled covalent intermediates. Using LC-MS under the negative ion mode, we captured single-charged and double-charged ion mass traces of the covalent intermediate of DK1–04 and NAD^+ (Supplementary Figure S5), confirming DK1–04 as a mechanism-based SIRT5 inhibitor.

Because JH-I5–2 and DK1–04 contain a free carboxylic acid, which might hinder cellular permeability, we developed two different pro-drug forms of these compounds: JH-I5–2am, JH-I5–2e, DK1–04am and DK1–04e (Figure 5C). The carboxylic acid is protected with either an acetomethoxy (am) or ethyl ester (e) group, which become hydrolyzed in cells to release the active SIRT5 inhibitors, JH-I5–2 and DK1–04. These pro-drug SIRT5 inhibitors were further used to evaluate drug efficacy in both cellular and *in vivo* settings.

SIRT5 prodrug inhibitors affect cancer cell growth *in vitro*.

The cellular cytotoxicity of the four pro-drug inhibitors was measured in 2D proliferation assays with MCF7 and MDA-MB-231 breast cancer cells. DK1–04am and DK1–04e showed greater cytotoxicity than JH-I5–2am and JH-I5–2e, which correlated with stronger *in vitro* SIRT5 inhibition by DK1–04 than JH-I5–2. In addition, the ethyl ester protected compound displayed greater cytotoxicity, as DK1–04e impeded cellular growth better than DK1–04am in breast cancer cells (Figure 6A). Among the four pro-drug inhibitors, DK1–04e showed the strongest cell growth inhibition. We also tested the two active forms of the SIRT5 inhibitors, JH-I5–2 and DK1–04. As expected, due to poor cell permeability, JH-I5–2 and DK1–04 did not affect cell proliferation. Furthermore, we tested the four pro-drug SIRT5 inhibitors in 2D cellular proliferation assays with various cancer cell lines, including lung (A549, NCI-H23), melanoma (B16-F10), colon (HCT-116) and pancreatic (CFPAC1) cancers. As in breast cancer cell lines, DK1–04e exhibited the strongest cytotoxicity, suggesting a broad anti-cancer effect (Supplementary Figure S6A). DK1–04am and DK1–04e, the inhibitors with strongest cytotoxicity, were less effective against non-tumorigenic HME1 mammary epithelial cells than MCF7 cells (Supplementary Figure S6B), suggesting that both compounds displayed cancer selectivity.

Given that genetic *SIRT5* targeting impaired anchorage-independent growth (Figure 2 and Supplementary Figure S2), we further tested the effect of the four pro-drug SIRT5 inhibitors on anchorage-independent growth. All four SIRT5 inhibitors potently suppressed the anchorage-independent growth of MCF7 and MDA-MB-231 breast cancer cells. Consistent with the cell proliferation assays, DK1–04 prodrugs showed slightly stronger effects than JH-I5–2, and DK1–04e showed stronger inhibition of anchorage-independent growth than DK1–04am (Figure 6B, C and Supplementary Figure S7). Thus, in both cell proliferation and anchorage-independent growth assays, targeting SIRT5 through either small molecule inhibitors or genetic perturbation similarly suppresses the transformed properties of breast cancer cells.

The effects of SIRT5 prodrug inhibitors on cancer cells are dependent on SIRT5 inhibition.

We next evaluated whether the compounds indeed inhibited SIRT5 in cells. All four compounds increased global lysine succinylation in MCF7 cells (Figure 6D). DK1–04e and DK1–04am, with stronger cytotoxicity, increased succinylation more than JH-I5–2am and JH-I5–2e. Also, the ethyl ester protected compounds showed stronger SIRT5 inhibition in MCF7 cells than the acetomethoxy protected compounds. Among the four SIRT5 inhibitors, DK1–04e displayed the strongest cytotoxicity and increased lysine succinylation the most. Thus, the effects of these inhibitors were tightly correlated with their ability to inhibit SIRT5. Both cytoplasmic and mitochondrial subcellular fractions exhibited significantly increased global succinylation after DK1–04e treatment, whereas the change was minimal in the nuclear fraction (Supplementary Figure S8). Consistent with the conclusion that the effects of DK1–04e resulted from SIRT5 inhibition, inhibitor treatment of MDA-MB-231 cells significantly increased mitochondrial oxidative stress (Supplementary Figure S4E), similar to the results from genetic *SIRT5* inactivation.

Next, we synthesized DK1–04(O) and DK1–04e(O) with oxygen replacing the sulfur in DK1–04 and DK1–04e, respectively (Figure 6E). Based on the mechanism of how these inhibitors work, we expected that DK1–04(O) would not inhibit SIRT5. As expected, DK1–04(O) did not inhibit SIRT5 desuccinylation activity even at 83.3 μM. Satisfyingly, in 2D proliferation assays, DK1–04e(O) caused much less cell cytotoxicity than DK1–04e in MCF7 (Figure 6F) or MDA-MB-231 (Supplementary Figure S6C) cells. Similarly, in soft agar assays, DK1–04e(O) was less effective compared to DK1–04e (Figure 6G). Finally, we tested DK1–04e on both parental *SIRT5* WT and *SIRT5*-targeted MDA-MB-231 clones. We hypothesized that *SIRT5* CRISPR/Cas9-editing would render MDA-MB-231 clones highly dependent on residual SIRT5 expression and therefore more vulnerable to SIRT5 inhibition. Indeed, DK1–04e caused greater cellular cytotoxicity in *SIRT5* targeted clones (Supplementary Figure S6D). Overall, these results support that SIRT5 inhibitory activity is important for the cellular cytotoxicity of DK1–04e.

SIRT5 inhibition suppresses mammary tumor growth in mouse models.

We next tested whether pharmacological SIRT5 inhibition could be useful for treating breast cancer *in vivo* using the MMTV-PyMT model. Upon initial mammary tumor palpation, female MMTV-PyMT mice received intraperitoneal (IP) injections of either the control vehicle (DMSO) or DK1–04e at 50 mg/kg, five times per week for 6 weeks. DK1–04e treatment reduced tumor burden when compared to vehicle treatment (Figure 7A). Total tumor weight was significantly lower in DK1–04e treated mice compared to controls (Figure 7B). Similar to results with genetic *Sirt5* inactivation, there were no significant differences in proliferation, mitotic figures or necrotic area between DK1–04e and vehicle-treated MMTV-PyMT mice (Supplementary Figure S9A-D). MMTV-PyMT mice treated with DK1–04e exhibited little alteration in metastasis as compared to vehicle control mice (Supplementary Figure S9E, F), perhaps because treatment was initiated upon tumor palpation, which may not be an early enough intervention to inhibit metastasis completely.

We detected the active SIRT5 inhibitor DK1–04 in serum, fat, and tumor, suggesting effective *in vivo* distribution, bioavailability, and stability. Importantly, DK1–04e treatment

did not cause apparent overt toxicity or body weight loss in mice (Figure 7C). Toxicity was further assessed by measurement of serum analytes from mice following chronic DK1–04e treatment, and the resulting data were within normal ranges, further indicating that the SIRT5 inhibitor is well tolerated (Supplementary Figure S9G). Finally, we addressed target engagement by evaluating global protein succinylation in DK1–04e-treated or control mammary tumors. Protein succinylation levels were substantially increased in tumors from DKI-04e treated mice, providing further evidence that DK1–04e treatment effectively reduced SIRT5 activity *in vivo* (Figure 7D). Another SIRT5 inhibitor prodrug, JH-I5–2am similarly inhibited tumor growth in MMTV-PyMT mice (Supplementary Figure S10). Together, these results indicate that pharmacological inhibition of SIRT5 has anticancer properties in the MMTV-PyMT model.

We further tested the SIRT5 inhibitor DK1–04e in a breast cancer cell line xenograft mouse model in which human MDA-MB-231 cells were subcutaneously injected into immunocompromised NSG mice. DK1–04e treatment (50 mg/kg, daily for 3 weeks) significantly reduced xenograft growth as well as overall tumor size and weight at endpoint (Figure 7E-G). There were no significant differences in tumor morphology, cell proliferation, or necrotic area between the two treatment groups (Supplementary Figure S9H-K). Consistent with the findings from the MMTV-PyMT mammary tumor model, DK1–04e did not cause any apparent toxicity or significant weight loss in mice with xenografts (Figure 7H). These results suggest that SIRT5 inhibitors have the potential to effectively treat breast cancer.

DISCUSSION

Elevated SIRT5 expression has been observed in a variety of cancers [16–18], and in breast cancer is associated with poor patient outcomes [19]. Here, we show that genetic or pharmacological SIRT5 disruption inhibited the anchorage-independent growth of cultured breast cancer cells and significantly reduced tumor progression *in vivo*, indicating that SIRT5 is an attractive candidate as a potential therapeutic target. SIRT5 functions as a de-acylase, and succinyl-lysine residues are one of its primary substrates [8, 11]. The process of protein succinylation is poorly understood but may be the product of a spontaneous reaction involving succinyl-CoA [47, 48]. SIRT5 is the only known mitochondrial desuccinylase, and many proteins in major metabolic pathways are modulated by SIRT5-regulated succinylation [10, 21, 24, 38, 49], including the TCA cycle, fatty acid metabolism, and amino acid degradation. These pathways provide energy and biosynthetic precursors, and their deregulation is associated with aberrant cancer cell proliferation [41, 50].

Our findings indicate that breast cancer cells are addicted to SIRT5 for anchorage-independent growth and suggest that the SIRT5-dependency is an example of non-oncogene addiction. Normal cells do not require SIRT5 for survival, whereas cancer cells have increased reliance on SIRT5, possibly because of their increased stress levels. Anchorage-independent growth causes increased ROS [40], rendering cells more reliant on mechanisms to remove ROS. We observed that a key enzyme for combatting ROS, IDH2, was hypersuccinylated upon *SIRT5* loss, suggesting that mitigating ROS via IDH2 may be one mechanism by which SIRT5 supports transformed cells. However, the phenotypic impact of

SIRT5 loss may represent the cumulative effect on multiple SIRT5 targets. Indeed, we previously reported that SIRT5-mediated desuccinylation stabilizes GLS in breast cancer cells and may thereby promote glutamine metabolism, which in several cancer contexts is important for cell proliferation or survival [39]. Even though most of our data focused on breast cancer, we observed that *SIRT5* inactivation inhibits several other types of cancer cells, possibly reflecting broad reliance on SIRT5 across several different cancers to combat oxidative stress.

Importantly, we demonstrated that pharmacological SIRT5 inhibition significantly reduced tumor growth in two different mouse models of breast cancer. Although SIRT5 inhibitors have previously been reported, most are limited by poor cell permeability and, to our knowledge, have not previously been tested *in vivo*. The SIRT5 inhibitors reported here demonstrate for the first time that pharmacological SIRT5 inhibition has promise as a mechanism-based strategy to treat cancer. Notably, *Sirt5* global knockout mice have only very mild phenotypes, including increased serum ammonia level [51] and cardiac hypertrophy in aged mice [38]. Likewise, SIRT5 inhibitors have modest effects on normal cells, and mice treated with SIRT5 inhibitors did not show signs of toxicity. These data suggest that SIRT5 is dispensable under normal conditions but required by cancer cells, highlighting its value as an actionable target in cancers. The SIRT5 inhibitors developed here will be useful tools to study SIRT5 functions and explore the therapeutic potential of targeting SIRT5.

MATERIALS AND METHODS

Antibodies and Immunoblotting.

As detailed in the Supplementary information, all antibodies were purchased from commercial sources, and immunoblotting was performed using standard approaches.

Mice.

All animals used in this study were handled in accordance with federal and institutional guidelines, under a protocol approved by the Cornell University Institutional Animal Care and Use Committee. Mice were housed under specific pathogen-free conditions in an Association for the Assessment and Accreditation of Laboratory Animal Care International accredited facility and cared for in compliance with the Guide for the Care and Use of Laboratory Animals.

Cell culture methods.

Cell culture conditions, preparation of mouse embryonic fibroblasts, cell immortalization, viral transduction, and CRISPR genome editing were conducted using standard approaches that are described in detail in the Supplementary information. Quantification of population doublings, 2D cellular viability, and soft agar growth was conducted using standard approaches described in the Supplementary information. Two to three independent experiments were performed for each measurement.

Monitoring mammary tumor development and tissue collection.

Sirt5$^{+/+}$ PyMT and *Sirt5*$^{-/-}$ PyMT female mice were palpated for tumors every other day beginning at 4 weeks of age. Detailed humane endpoint criteria and methods for euthanasia, tissue collection, and histopathological analysis, as well as methods for SIRT5 inhibitor treatment of mice, are provided in the Supplementary information.

Succinylation proteomics.

Frozen powdered mammary tumor tissues from 4 *Sirt5*$^{+/+}$ PyMT and 4 *Sirt5*$^{-/-}$ PyMT mice were homogenized, lysed, and analyzed by Nano LC-MS/MS for the identification and quantification of succinyl-lysine peptides as previously described [38].

High performance liquid chromatography for GSH and NADP^{+}/NADPH measurement.

Intracellular glutathione and NADP^{+}/NADPH levels were determined using standard methods; additional experimental details are provided in the Supplementary information. Three independent experiments were performed for each measurement.

Measurement of reactive oxygen species.

MDA-MB-231 or HCT116 cells in triplicate were incubated with 7-Amino-Actinomycin D (BD Bioscience), stained with CM-H2DCFDA or MitoSOX Red (Thermo Fisher Scientific), and analyzed by flow cytometry. Three to four independent experiments were performed for each measurement.

Syntheses and characterization of various SIRT5 inhibitors.

Detailed descriptions of compound synthesis and characterization are provided in the Supplementary information.

Cloning, expression and purification of SIRT1, 2, 3, 5 and 6.

Human SIRT1, SIRT2, SIRT3 and SIRT5 were cloned, expressed and purified as previously reported [45, 52].

Deacetylase, desuccinylase activity assays of SIRT1, 2, 3, 5 and 6.

To measure the *in vitro* IC_{50} values of the synthesized inhibitors on SIRT1, 2, 3, 5 and 6 previously reported procedure was followed (n = 3, biological replicates) [45, 52].

Preparation of Ac-H3K9, Succinyl-H3K9 peptides.

The sequence of Ac-H3K9 peptide for de-acetylase sirtuin enzymatic assay was KQTAR-(Ac-K)-STGGWW. The sequence of Succinyl-H3K9 peptide was KQTAR-(Succinyl-K)-STGGWW. Both were synthesized by FOCUS peptide synthesizer, as previously reported [45].

Supplementary Material

Refer to Web version on PubMed Central for supplementary material.

ACKNOWLEDGMENTS

The authors thank the NCI Physical Sciences-Oncology Network Bioresource Core Facility (PBCF) for MDA-MB-231 cells, and Drs. Ruchika Bhawal and Sheng Zhang from the Cornell Proteomics and Metabolomics Facility for technical assistance. This work was supported in part by NIH R01 grants CA163255 and CA223534. Y.L.N.A was supported by NIH/NIGMS grant 5T32GM008500, and I.R.F was supported by NIH/NIGMS grant T32GM007273, a Cornell Deans Excellence Fellowship, and a HHMI Gilliam Fellowship. JA was supported by grants from the Ecole Polytechnique Federale de Lausanne (EPFL), and the Swiss National Science Foundation (SNSF 31003A_179435). This work utilized the Cornell University NMR facility, which is supported in part by the NSF through MRI award CHE-1531632.

REFERENCES

1. Harbeck N, Penault-Llorca F, Cortes J, Gnant M, Houssami N, Poortmans P et al. Breast cancer. Nat Rev Dis Primers 2019; 5: 66. [PubMed: 31548545]
2. Unterlass JE, Curtin NJ. Warburg and Krebs and related effects in cancer. Expert Rev Mol Med 2019; 21: e4. [PubMed: 31558177]
3. Hirschey MD, Zhao Y. Metabolic Regulation by Lysine Malonylation, Succinylation, and Glutarylation. Molecular & cellular proteomics : MCP 2015; 14: 2308–2315. [PubMed: 25717114]
4. Lin H, Su X, He B. Protein lysine acylation and cysteine succination by intermediates of energy metabolism. ACS Chem Biol 2012; 7: 947–960. [PubMed: 22571489]
5. Bheda P, Jing H, Wolberger C, Lin H. The Substrate Specificity of Sirtuins. Annual review of biochemistry 2016; 85: 405–429.
6. Houtkooper RH, Pirinen E, Auwerx J. Sirtuins as regulators of metabolism and healthspan. Nat Rev Mol Cell Biol (10.1038/nrm3293) 2012; 13: 225–238. [PubMed: 22395773]
7. Imai S-i, Armstrong CM, Kaeberlein M, Guarente L. Transcriptional silencing and longevity protein Sir2 is an NAD-dependent histone deacetylase. Nature 2000; 403: 795–800. [PubMed: 10693811]
8. Du J, Zhou Y, Su X, Yu J, Khan S, Jiang H et al. Sirt5 is an NAD-dependent protein lysine demalonylase and desuccinylase. Science 2011; 334: 806–809. [PubMed: 22076378]
9. Nishida Y, Rardin MJ, Carrico C, He W, Sahu AK, Gut P et al. SIRT5 Regulates both Cytosolic and Mitochondrial Protein Malonylation with Glycolysis as a Major Target. Molecular cell 2015; 59: 321–332. [PubMed: 26073543]
10. Park J, Chen Y, Tishkoff DX, Peng C, Tan M, Dai L et al. SIRT5-mediated lysine desuccinylation impacts diverse metabolic pathways. Mol Cell 2013; 50: 919–930. [PubMed: 23806337]
11. Peng C, Lu Z, Xie Z, Cheng Z, Chen Y, Tan M et al. The first identification of lysine malonylation substrates and its regulatory enzyme. Molecular & cellular proteomics : MCP 2011; 10: M111 012658. [PubMed: 21908771]
12. Tan M, Peng C, Anderson KA, Chhoy P, Xie Z, Dai L et al. Lysine glutarylation is a protein posttranslational modification regulated by SIRT5. Cell metabolism 2014; 19: 605–617. [PubMed: 24703693]
13. Finley LWS, Carracedo A, Lee J, Souza A, Egia A, Zhang J et al. SIRT3 opposes reprogramming of cancer cell metabolism through HIF1[alpha] destabilization. Cancer Cell 2011; 19: 416–428. [PubMed: 21397863]
14. Polletta L, Vernucci E, Carnevale I, Arcangeli T, Rotili D, Palmerio S et al. SIRT5 regulation of ammonia-induced autophagy and mitophagy. Autophagy 2015; 11: 253–270. [PubMed: 25700560]
15. Sebastián C, Zwaans BMM, Silberman DM, Gymrek M, Goren A, Zhong L et al. The histone deacetylase SIRT6 is a tumor suppressor that controls cancer metabolism. Cell 2012; 151: 1185–1199. [PubMed: 23217706]
16. Chang L, Xi L, Liu Y, Liu R, Wu Z, Jian Z. SIRT5 promotes cell proliferation and invasion in hepatocellular carcinoma by targeting E2F1. Molecular medicine reports 2018; 17: 342–349. [PubMed: 29115436]
17. Igci M, Kalender ME, Borazan E, Bozgeyik I, Bayraktar R, Bozgeyik E et al. High-throughput screening of Sirtuin family of genes in breast cancer. Gene 2016; 586: 123–128. [PubMed: 27080717]

18. Lu W, Zuo Y, Feng Y, Zhang M. SIRT5 facilitates cancer cell growth and drug resistance in non-small cell lung cancer. Tumour biology : the journal of the International Society for Oncodevelopmental Biology and Medicine 2014; 35: 10699–10705. [PubMed: 25070488]
19. Xu L, Che X, Wu Y, Song N, Shi S, Wang S et al. SIRT5 as a biomarker for response to anthracycline-taxane-based neoadjuvant chemotherapy in triple-negative breast cancer. Oncol Rep 2018; 39: 2315–2323. [PubMed: 29565454]
20. Wang YQ, Wang HL, Xu J, Tan J, Fu LN, Wang JL et al. Sirtuin5 contributes to colorectal carcinogenesis by enhancing glutaminolysis in a deglutarylation-dependent manner. Nature communications 2018; 9: 545.
21. Xiangyun Y, Xiaomin N, Linping G, Yunhua X, Ziming L, Yongfeng Y et al. Desuccinylation of pyruvate kinase M2 by SIRT5 contributes to antioxidant response and tumor growth. Oncotarget 2017; 8: 6984–6993. [PubMed: 28036303]
22. Yang X, Wang Z, Li X, Liu B, Liu M, Liu L et al. SHMT2 Desuccinylation by SIRT5 Drives Cancer Cell Proliferation. Cancer research 2018; 78: 372–386. [PubMed: 29180469]
23. Lin ZF, Xu HB, Wang JY, Lin Q, Ruan Z, Liu FB et al. SIRT5 desuccinylates and activates SOD1 to eliminate ROS. Biochem Biophys Res Commun 2013; 441: 191–195. [PubMed: 24140062]
24. Zhou L, Wang F, Sun R, Chen X, Zhang M, Xu Q et al. SIRT5 promotes IDH2 desuccinylation and G6PD deglutarylation to enhance cellular antioxidant defense. EMBO reports 2016; 17: 811–822. [PubMed: 27113762]
25. He B, Du J, Lin H. Thiosuccinyl peptides as Sirt5-specific inhibitors. J Am Chem Soc 2012; 134: 1922–1925. [PubMed: 22263694]
26. Jiang Y, Zheng W. Cyclic tripeptide-based potent and selective human SIRT5 inhibitors. Medicinal chemistry (Shariqah (United Arab Emirates)) 2019.
27. Kalbas D, Liebscher S, Nowak T, Meleshin M, Pannek M, Popp C et al. Potent and Selective Inhibitors of Human Sirtuin 5. Journal of medicinal chemistry 2018; 61: 2460–2471. [PubMed: 29494161]
28. Liu J, Huang Y, Zheng W. A Selective Cyclic Peptidic Human SIRT5 Inhibitor. Molecules (Basel, Switzerland) 2016; 21.
29. Maurer B, Rumpf T, Scharfe M, Stolfa DA, Schmitt ML, He W et al. Inhibitors of the NAD+-dependent protein desuccinylase and demalonylase Sirt5. ACS Med Chem Lett 2012; 3: 1050–1053. [PubMed: 24900427]
30. Rajabi N, Auth M, Troelsen KR, Pannek M, Bhatt DP, Fontenas M et al. Mechanism-Based Inhibitors of the Human Sirtuin 5 Deacylase: Structure-Activity Relationship, Biostructural, and Kinetic Insight. Angewandte Chemie (International ed in English) 2017; 56: 14836–14841. [PubMed: 29044784]
31. Gao J, Aksoy BA, Dogrusoz U, Dresdner G, Gross B, Sumer SO et al. Integrative analysis of complex cancer genomics and clinical profiles using the cBioPortal. Sci Signal 2013; 6: pl1.
32. Ciriello G, Gatza ML, Beck AH, Wilkerson MD, Rhie SK, Pastore A et al. Comprehensive Molecular Portraits of Invasive Lobular Breast Cancer. Cell 2015; 163: 506–519. [PubMed: 26451490]
33. Jackson EL, Willis N, Mercer K, Bronson RT, Crowley D, Montoya R et al. Analysis of lung tumor initiation and progression using conditional expression of oncogenic K-ras. Genes Dev 2001; 15: 3243–3248. [PubMed: 11751630]
34. Guy CT, Cardiff RD, Muller WJ. Induction of mammary tumors by expression of polyomavirus middle T oncogene: a transgenic mouse model for metastatic disease. Mol Cell Biol 1992; 12: 954–961. [PubMed: 1312220]
35. Herschkowitz JI, Simin K, Weigman VJ, Mikaelian I, Usary J, Hu Z et al. Identification of conserved gene expression features between murine mammary carcinoma models and human breast tumors. Genome biology 2007; 8: R76. [PubMed: 17493263]
36. Lin EY, Jones JG, Li P, Zhu L, Whitney KD, Muller WJ et al. Progression to malignancy in the polyoma middle T oncoprotein mouse breast cancer model provides a reliable model for human diseases. The American journal of pathology 2003; 163: 2113–2126. [PubMed: 14578209]

37. Cardiff RD, Anver MR, Gusterson BA, Hennighausen L, Jensen RA, Merino MJ et al. The mammary pathology of genetically engineered mice: the consensus report and recommendations from the Annapolis meeting. Oncogene 2000; 19: 968–988. [PubMed: 10713680]
38. Sadhukhan S, Liu X, Ryu D, Nelson OD, Stupinski JA, Li Z et al. Metabolomics-assisted proteomics identifies succinylation and SIRT5 as important regulators of cardiac function. Proc Natl Acad Sci U S A 2016; 113: 4320–4325. [PubMed: 27051063]
39. Greene KS, Lukey MJ, Wang X, Blank B, Druso JE, Lin MJ et al. SIRT5 stabilizes mitochondrial glutaminase and supports breast cancer tumorigenesis. Proc Natl Acad Sci U S A 2019.
40. Schafer ZT, Grassian AR, Song L, Jiang Z, Gerhart-Hines Z, Irie HY et al. Antioxidant and oncogene rescue of metabolic defects caused by loss of matrix attachment. Nature 2009; 461: 109–113. [PubMed: 19693011]
41. Jiang L, Shestov AA, Swain P, Yang C, Parker SJ, Wang QA et al. Reductive carboxylation supports redox homeostasis during anchorage-independent growth. Nature 2016; 532: 255–258. [PubMed: 27049945]
42. Kalyanaraman B, Darley-Usmar V, Davies KJ, Dennery PA, Forman HJ, Grisham MB et al. Measuring reactive oxygen and nitrogen species with fluorescent probes: challenges and limitations. Free Radic Biol Med 2012; 52: 1–6. [PubMed: 22027063]
43. Farooqi AS, Hong JY, Cao J, Lu X, Price IR, Zhao Q et al. Novel Lysine-Based Thioureas as Mechanism-Based Inhibitors of Sirtuin 2 (SIRT2) with Anticancer Activity in a Colorectal Cancer Murine Model. Journal of medicinal chemistry 2019; 62: 4131–4141. [PubMed: 30986062]
44. Spiegelman NA, Hong JY, Hu J, Jing H, Wang M, Price IR et al. A Small-Molecule SIRT2 Inhibitor That Promotes K-Ras4a Lysine Fatty-Acylation. ChemMedChem 2019; 14: 744–748. [PubMed: 30734528]
45. Jing H, Hu J, He B, Negrón Abril YL, Stupinski J, Weiser K et al. A SIRT2-Selective Inhibitor Promotes c-Myc Oncoprotein Degradation and Exhibits Broad Anticancer Activity. Cancer Cell 2016; 29: 297–310. [PubMed: 26977881]
46. Smith BC, Denu JM. Mechanism-based Inhibition of Sir2 deacetylases by thioacetyl-lysine peptide. Biochemistry 2007; 46: 14478–14486. [PubMed: 18027980]
47. Wagner GR, Bhatt DP, O'Connell TM, Thompson JW, Dubois LG, Backos DS et al. A Class of Reactive Acyl-CoA Species Reveals the Non-enzymatic Origins of Protein Acylation. Cell metabolism 2017; 25: 823–837 e828. [PubMed: 28380375]
48. Wagner GR, Hirschey MD. Nonenzymatic protein acylation as a carbon stress regulated by sirtuin deacylases. Molecular cell 2014; 54: 5–16. [PubMed: 24725594]
49. Rardin MJ, He W, Nishida Y, Newman JC, Carrico C, Danielson SR et al. SIRT5 Regulates the Mitochondrial Lysine Succinylome and Metabolic Networks. Cell metabolism 2013; 18: 920–933. [PubMed: 24315375]
50. Phan LM, Yeung SC, Lee MH. Cancer metabolic reprogramming: importance, main features, and potentials for precise targeted anti-cancer therapies. Cancer Biol Med 2014; 11: 1–19. [PubMed: 24738035]
51. Yu J, Sadhukhan S, Noriega LG, Moullan N, He B, Weiss RS et al. Metabolic characterization of a Sirt5 deficient mouse model. Sci Rep 2013; 3: 2806. doi: 10.1038/srep02806. [PubMed: 24076663]
52. Spiegelman NA, Price IR, Jing H, Wang M, Yang M, Cao J et al. Direct Comparison of SIRT2 Inhibitors: Potency, Specificity, Activity-Dependent Inhibition, and On-Target Anticancer Activities. ChemMedChem 2018; 13: 1890–1894. [PubMed: 30058233]

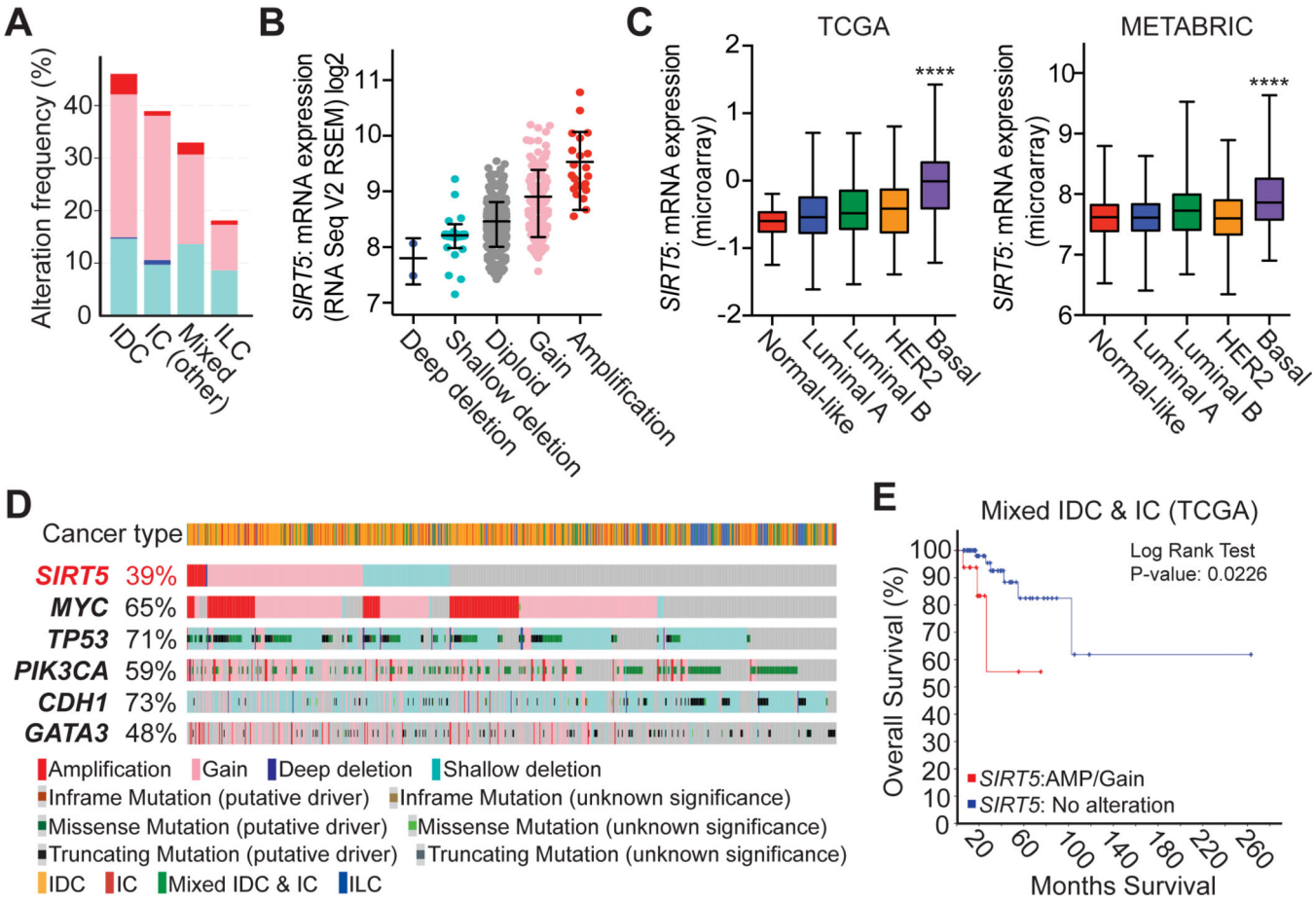

Figure 1. SIRT5 is overexpressed in human breast cancer.

(A) *SIRT5* copy number alteration (amplification (red), gain (pink), deep deletion (blue), shallow deletion (aqua blue)) across different histopathological breast cancer subtypes: invasive ductal carcinoma (IDC), invasive lobular carcinoma (ILC), mixed ductal/lobular (Mixed), and other invasive carcinoma types (IC (other)). **(B)** *SIRT5* mRNA expression levels (determined by RNA-seq) with respect to relative DNA copy-number alterations in TCGA breast cancers. Results from the query (SIRT5: AMP GAIN MUT HOMDEL HETLOSS) were analyzed and plotted using the TCGA dataset (n = 817) in cBioPortal. Presented data are the mean values ± standard deviation. **(C)** *SIRT5* mRNA expression levels (determined by microarray) across breast invasive carcinoma subtypes classified by Pam50: normal-like, luminal A, luminal B, HER2-enriched and basal. Results from the query described above were analyzed and plotted using the TCGA (n = 481 total, n = 8 normal-like, n = 212 luminal-A, n = 119 luminal-B, n = 55 HER2-enriched, n = 87 basal) and METABRIC (n = 1669 total, n = 140 normal-like, n = 679 luminal-A, n = 461 luminal-B, n = 220 HER2-enriched, n = 199 basal) datasets in cBioPortal (* means p value <0.0001, One-way ANOVA, Tukey's multiple comparisons test). **(D)** Genetic alterations of *SIRT5* and recurrently altered genes: *MYC*, *TP53*, *PIK3CA*, *CDH1*, *GATA3* in breast invasive carcinomas. Values in the left of the diagram reflect the total percentage of copy number alterations for the corresponding gene across 817 breast invasive carcinoma samples. Results from the query (GENE: MUT AMP HOMDEL GAIN HETLOSS) were analyzed and

plotted using the TCGA dataset in cBioPortal. **(E)** Kaplan-Meier curves comparing the overall survival of patients with and without amplification or gain of *SIRT5* copy number across the mixed histology subpopulation. Results from the query (SIRT5: AMP GAIN) were analyzed and plotted using the TCGA dataset (n = 88, mixed histology subtype) in cBioPortal (p value = 0.0226, Log Rank Test).

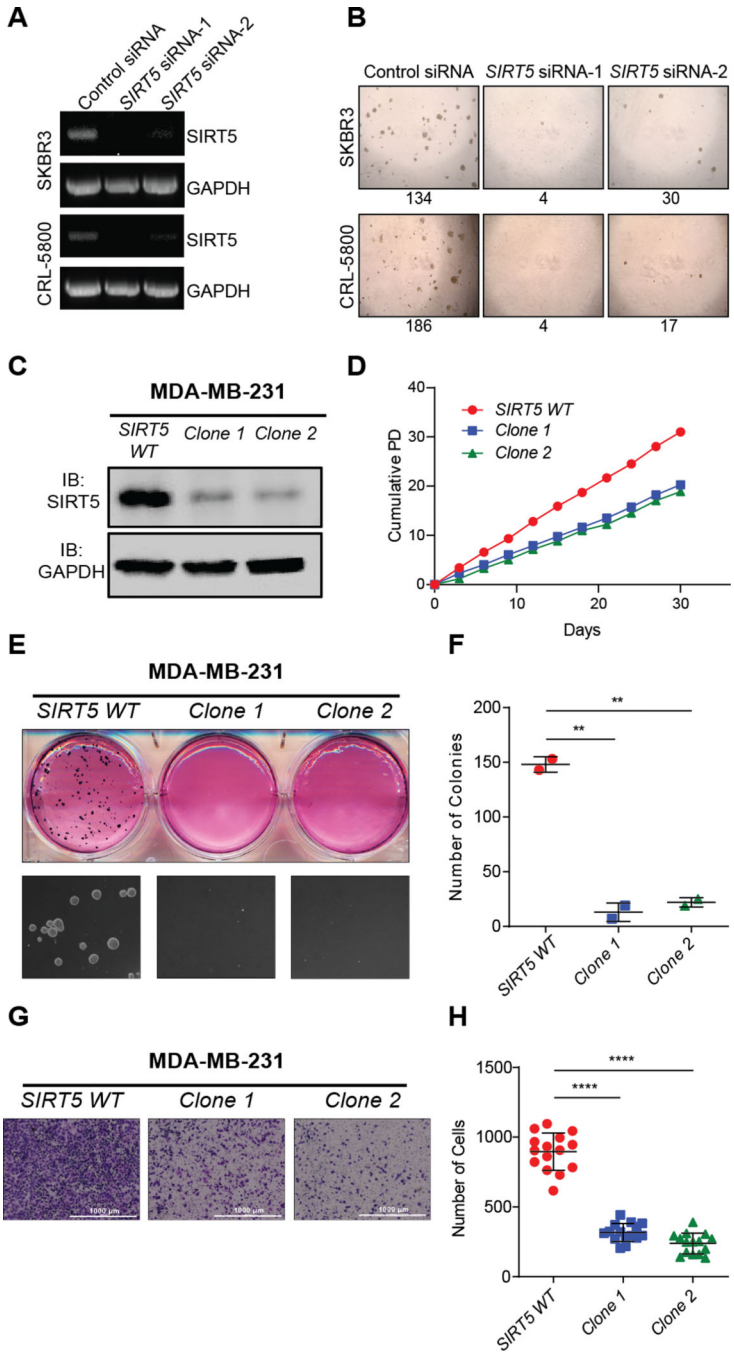

Figure 2. *Sirt5* knock-down inhibits the anchorage-independent growth of human cancer cells.

(A) Gel image of RT-PCR products for *SIRT5* and *GAPDH* as loading control, showing effective *SIRT5* knockdown by two different siRNA in SKBR3 (breast cancer) and CRL-5800 (lung cancer) cells. **(B)** Representative images of soft-agar assay demonstrating that *SIRT5* knockdown inhibits colony formation in SKBR3 and CRL-5800 cancer cells. Number of colonies counted is shown below the images. **(C)** Immunoblot for SIRT5 and GAPDH as a loading control in parental *SIRT5* WT MDA-MB-231 cells and CRISPR/Cas9-edited *SIRT5* clones 1 and 2 (n = 3 independent experiments). **(D)** Population doubling

analysis of MDA-MB-231 cells, comparing the proliferation of parental *SIRT5* WT cells and CRISPR/Cas9-edited *SIRT5* clones 1 and 2. **(E)** Representative images for soft agar growth assay with the parental *SIRT5* WT cells and CRISPR/Cas9-edited *SIRT5* clones 1 and 2. **(F)** Quantification of colony numbers in soft agar assays with parental *SIRT5* WT cells and CRISPR/Cas9-edited *SIRT5* clones 1 and 2. Data are presented as mean values ± standard deviation (** P value < 0.01, Unpaired t-test, n = 2 independent experiments). **(G)** Representative images from invasion assays using a Boyden chamber coated with matrigel, comparing MDA-MB-231 parental *SIRT5* WT cells and CRISPR/Cas9-edited *SIRT5* clones 1 and 2. **(H)** Quantification of MDA-MB-231 cell migration in the invasion assay. Data are presented as mean values ± standard deviation (**** P value < 0.0001, Unpaired t-test, n = 3 independent experiments).

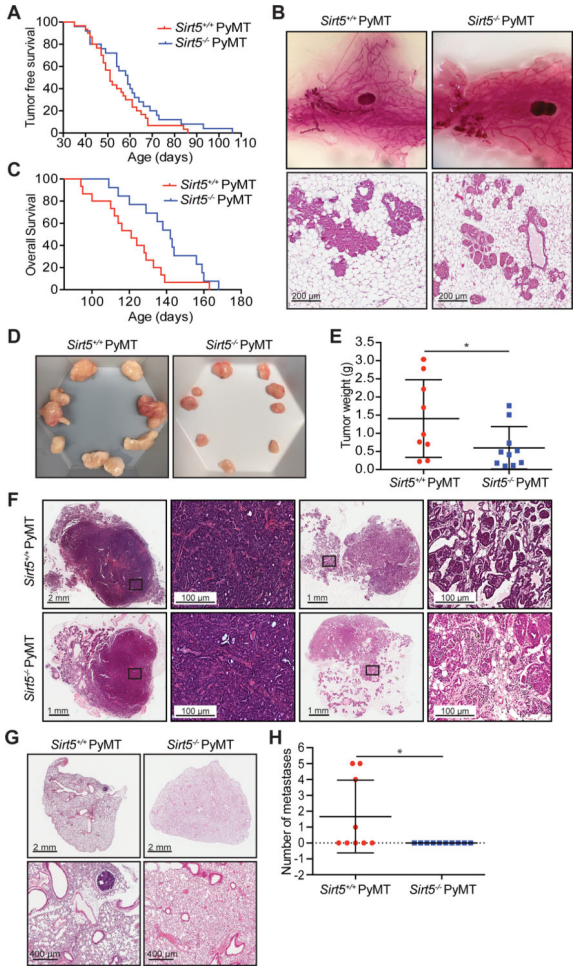

Figure 3. *Sirt5* deletion impairs tumor growth and reduces metastasis burden *in vivo*.

(A) Kaplan Meier tumor free survival curve for *Sirt5*$^{+/+}$ PyMT (n = 30) and *Sirt5*$^{-/-}$ PyMT (n = 25) mice. A slight delay in mammary tumor development was observed in *Sirt5*$^{-/-}$ PyMT mice (P value = 0.1352, Log Rank (Mantel-Cox test)). **(B)** Representative carmine alum and H&E-stained whole mammary glands from 42 days old *Sirt5*$^{+/+}$ PyMT (n = 3) and *Sirt5*$^{-/-}$ PyMT mice (n = 4). **(C)** Kaplan Meier overall survival curve for *Sirt5*$^{+/+}$ PyMT (n = 15) and *Sirt5*$^{-/-}$ PyMT (n =13) mice. Prolonged survival was observed in *Sirt5*$^{-/-}$ PyMT mice (P value = 0.0256, Log Rank (Mantel-Cox test)). **(D)** Representative images of mammary tumors collected fifty days after palpation of the first tumor in *Sirt5*$^{+/+}$ PyMT (n = 9) and *Sirt5*$^{-/-}$ PyMT (n = 10) mice. **(E)** Total tumor weight for the same *Sirt5*$^{+/+}$ PyMT and *Sirt5*$^{-/-}$ PyMT mice. Data are presented as the mean values ± standard deviation, (* P value = 0.0435, Mann-Whitney test). **(F)** Representative hematoxylin and eosin (H&E) staining of mammary tumor sections from *Sirt5*$^{+/+}$ PyMT (n = 9) and *Sirt5*$^{-/-}$ PyMT (n = 10) mice. Tumors were harvested 50 days after initial tumor detection. Scale bars represent 2 mm, 1 mm and 100 µm. **(G)** Representative images of lung tissues from *Sirt5*$^{+/+}$ PyMT (n = 9) and *Sirt5*$^{-/-}$ PyMT (n = 10) mice. Scale bars represent 2 mm and 400 µm. **(H)** Quantification of number of foci observed in lung tissues from *Sirt5*$^{+/+}$ PyMT (n = 9) and *Sirt5*$^{-/-}$ PyMT (n = 10) mice. Presented data are the mean values ± standard deviation, (* P value = 0.0339,

Unpaired t-test). Lung tissue was harvested 50 days after initial tumor detection and 5 H&E slides were analyzed per mouse.

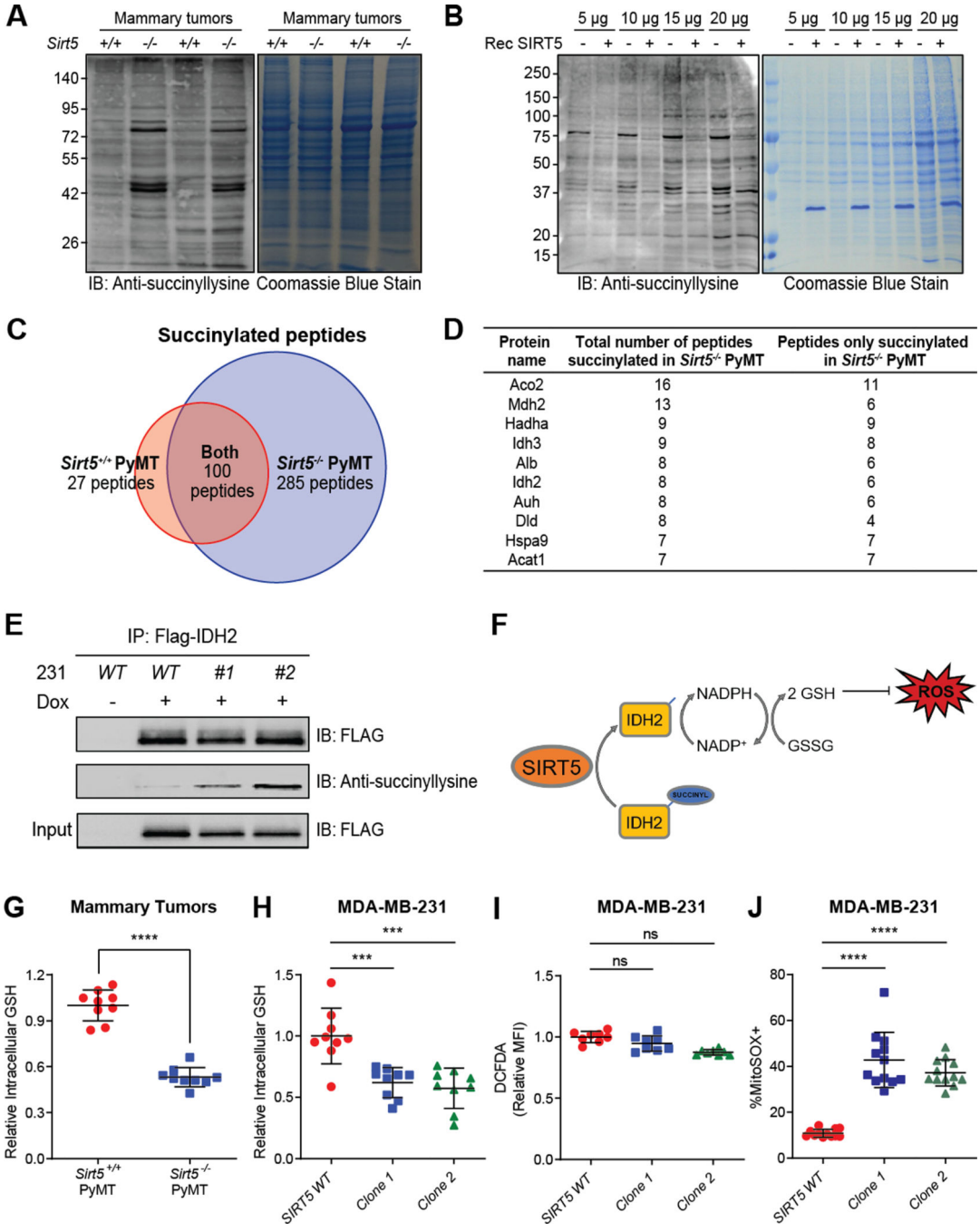

Figure 4. *Sirt5* deletion significantly increases succinylation levels of proteins and increases ROS levels.

(A) Immunoblot of mammary tumor lysates with anti-succinyllysine antibody. Tissue lysates were prepared using tumor tissues from mice that were euthanized 50 days after initial tumor detection. Tumor tissues from *Sirt5*$^{-/-}$ PyMT mice showed increased succinylation levels when compared to *Sirt5*$^{+/+}$ PyMT. Coomassie blue staining was used as a loading control. **(B)** *In-vitro* reaction of SIRT5 with mammary tumor extracts from *Sirt5*$^{-/-}$ PyMT mice. Recombinant (Rec) SIRT5 was added into a mixture containing 5, 10, 15 or 20 µg of

tumor lysate from a *Sirt5*$^{-/-}$ PyMT mouse and incubated at 45 °C for an hour. Western blotting with an anti-succinyllysine antibody was used to examine succinylation levels. Reduced succinylation was observed upon SIRT5 treatment. Coomassie blue staining was used as a loading control. **(C)** Venn diagram showing the number of unique succinylated peptides identified in the proteomics studies performed with *Sirt5*$^{+/+}$ PyMT and *Sirt5*$^{-/-}$ PyMT mammary tumors (4 mice per genotype). **(D)** List of the top ten proteins with the highest number of succinylated peptides in *Sirt5*$^{-/-}$ PyMT mammary tumors. **(E)** Immunoprecipitation of ectopically expressed FLAG-tagged wild-type IDH2 from lysates of MDA-MB-231 parental *SIRT5* WT cells and CRISPR/Cas9-edited *SIRT5* clones 1 and 2 followed by western blot analysis using an anti-succinyllysine antibody. **(F)** Schematic of SIRT5-mediated regulation of IDH2. **(G)** Intracellular glutathione (GSH) levels of mammary tumors collected fifty days after initial tumor detection in *Sirt5*$^{-/-}$ PyMT mice relative to *Sirt5*$^{+/+}$ PyMT controls (* P value = 0.0150, Unpaired t-test, n = 3 for each group). **(H)** Intracellular glutathione levels in CRISPR/Cas9 edited MDA-MB-231 clones 1 and 2 relative to *SIRT5* WT parental cells. Glutathione levels were determined by HPLC. (*** P value = 0.0008, *** P value = 0.0004, Unpaired t-test, n = 3 technical replicates, in 3 independent experiments). **(I)** Median fluorescence intensity (MFI) quantification of DCFDA in MDA-MB-231 clones 1 and 2 relative to *SIRT5* WT parental cells. No statistical differences were observed. (P = 0.0827, P = 0.0724, Unpaired t-test, n = 4 technical replicates, in 2 independent experiments). **(J)** Quantification of MitoSOX positive cells in MDA-MB-231 clones 1 and 2 relative to *SIRT5* WT parental cells. (*** P = 0.0002, * P = 0.0319, Unpaired t-test, n = 4 technical replicates, in 2 independent experiments). DCFDA and MitoSOX were measured by flow cytometry. Data are presented in panels G to J as mean values ± standard deviation.

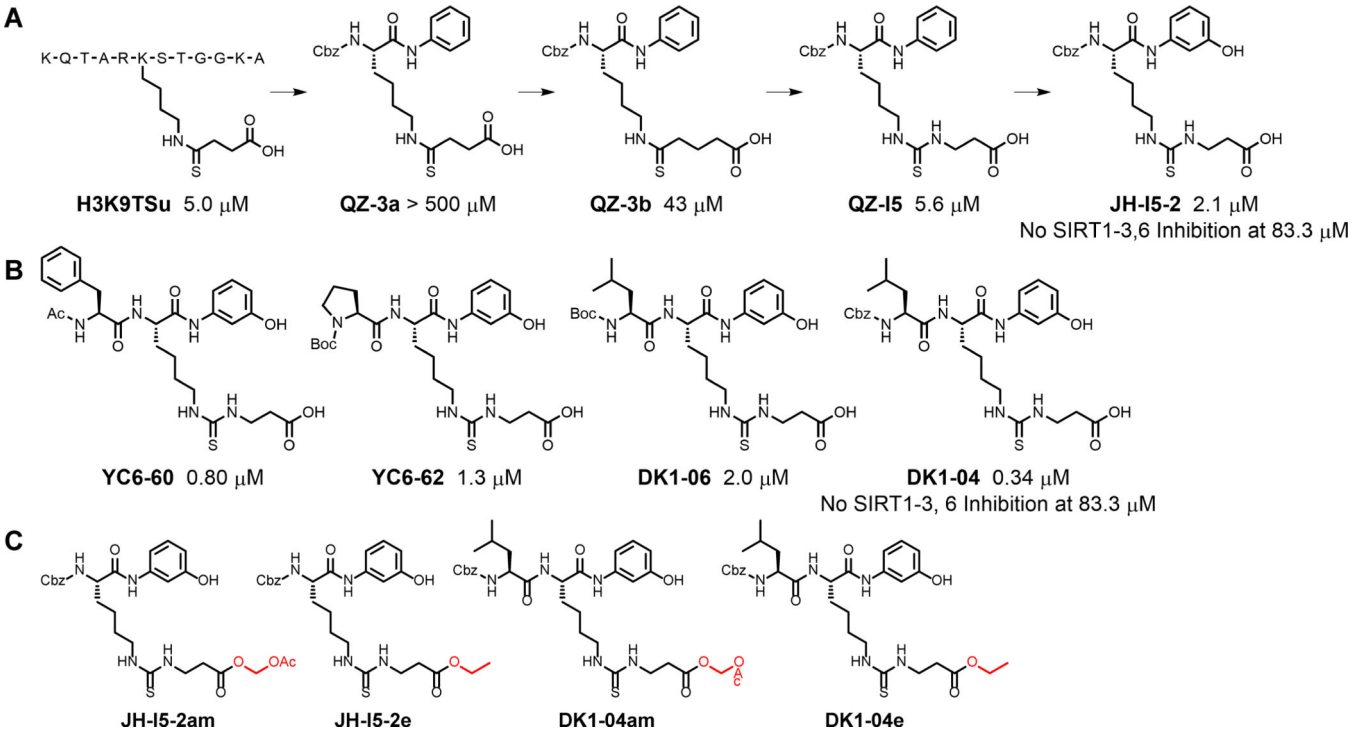

Figure 5. Development of thiourea SIRT5 inhibitors JH-I5-2 and DK1-04.

(A) The development of JH-I5-2 from a peptide-based inhibitor H3K9TSu. The *in vitro* IC50 value of each compound is indicated (n = 3 biological replicates). **(B)** Structures of four dipeptide-based SIRT5 inhibitors developed. **(C)** Structures of prodrug forms of JH-I5-2 and DK1-04.

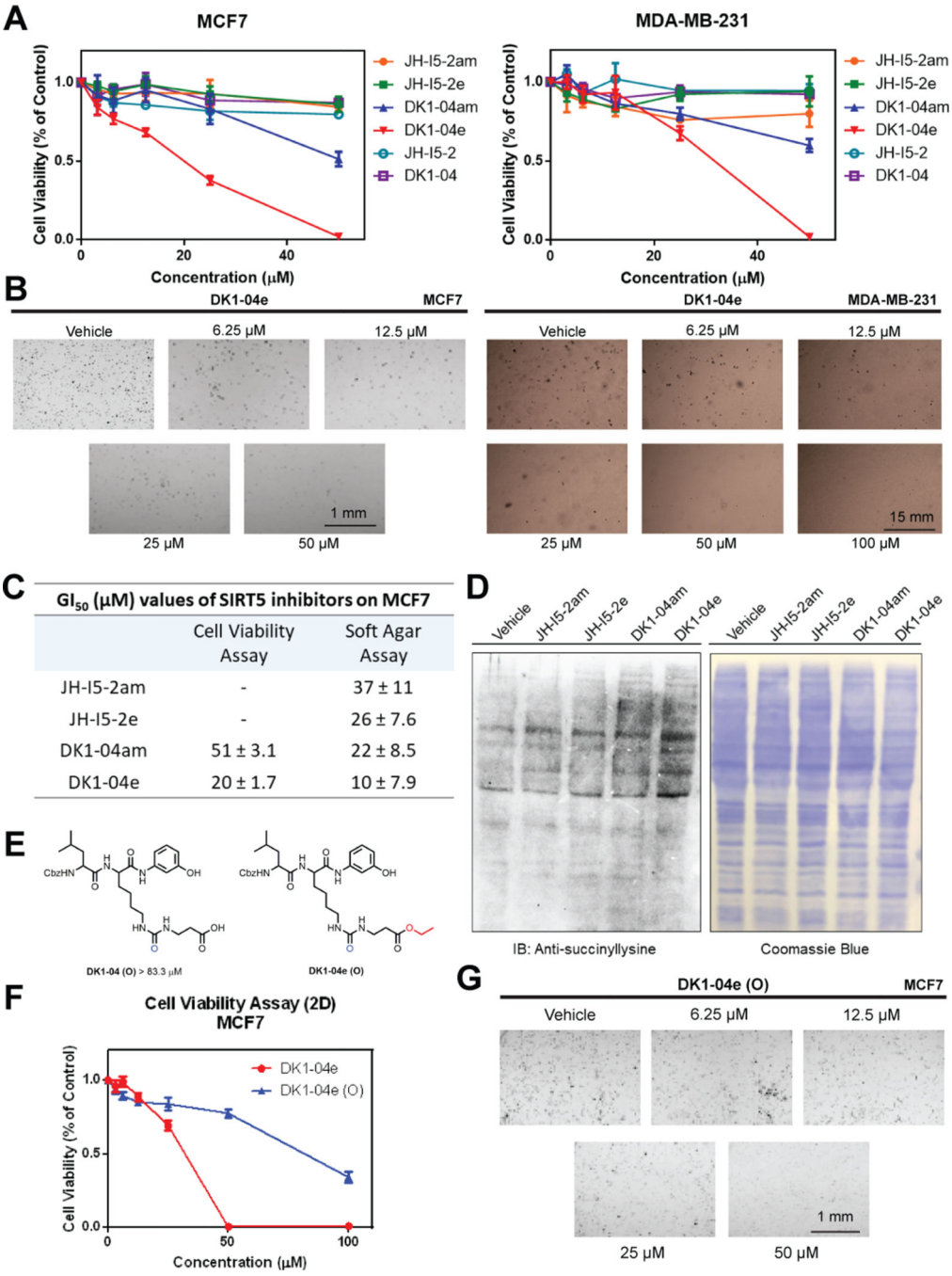

Figure 6. DK1-04e inhibits the cellular growth of breast cancer cells by targeting SIRT5.

(A) Cellular proliferation assay with MCF7 and MDA-MB-231 cells treated with indicated inhibitors for 72 hours (n = 3 technical replicates). **(B)** Soft agar colony formation assay of MCF7 and MDA-MB-231 cells treated with DK1-04e for 10 days. **(C)** GI_{50} values of the four SIRT5 inhibitor prodrugs for MCF7 cells in cell viability and soft agar assays (n = 3 technical replicates). **(D)** Immunoblots of global lysine succinylation of MCF7 cells treated with 50 μM of indicated inhibitors for 24 hours. Coomassie blue staining was used as a loading control. **(E)** Structures of the negative control compounds, DK1-04(O) and

DK1-04e(O). **(F)** Cellular proliferation assay of MCF7 cells treated with DK1-04e(O) for 72 hours (n = 3 technical replicates). **(G)** Soft agar colony formation assay of MCF7 cells treated with DK1-04e(O) for 10 days.

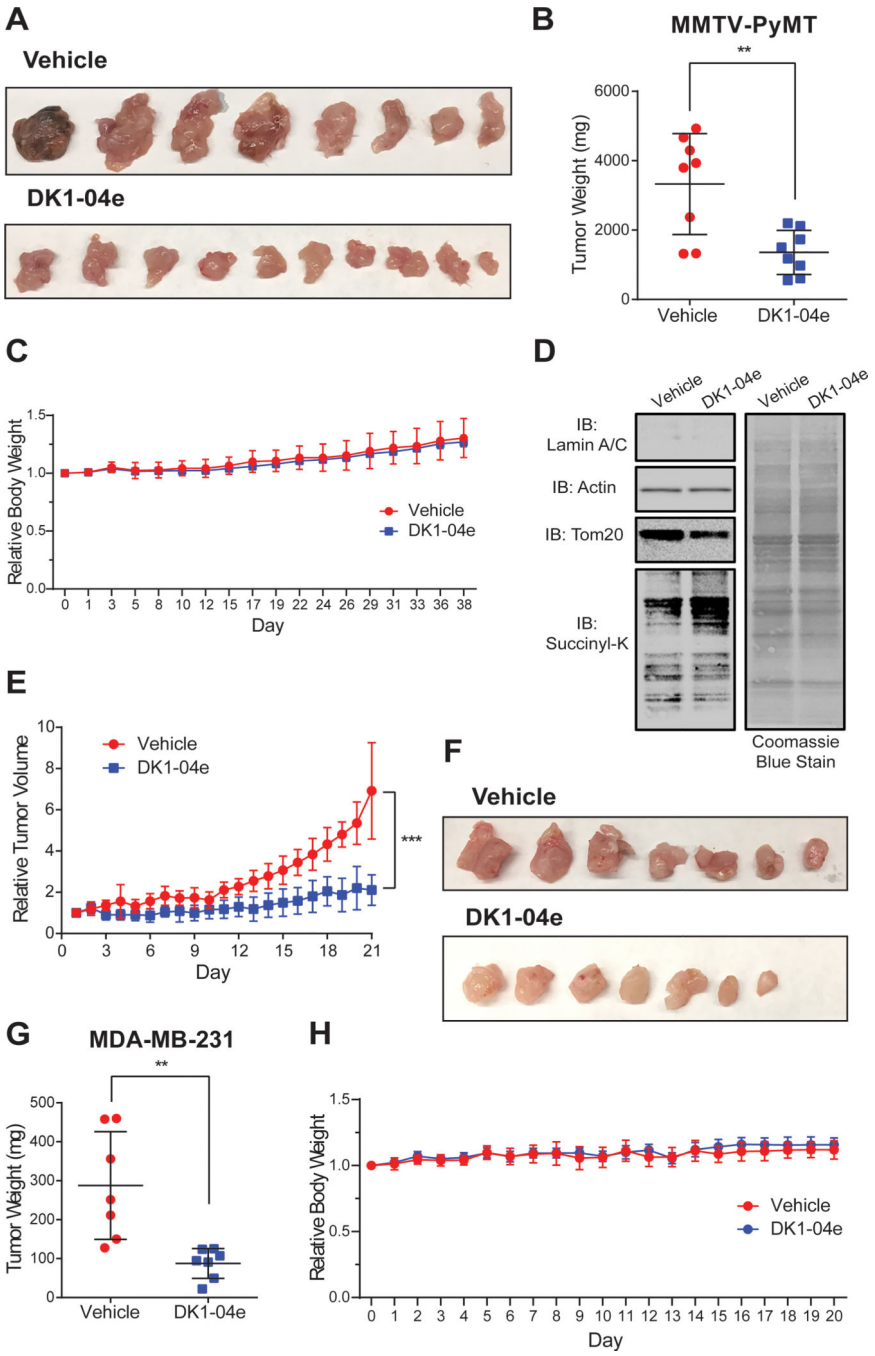

Figure 7. SIRT5-selective inhibitor DK1-04e impairs mammary tumor growth in MMTV-PyMT transgenic mice and human breast cancer mouse model.

(A) Representative images and **(B)** total tumor weight of mammary tumors from MMTV-PyMT mice that were treated 5 times per week for 6 weeks with 50 mg/kg DK1-04e (n = 8) or vehicle (n = 8) upon initial tumor detection. MMTV PyMT mice treated with DK1-04e showed reduced tumor weight as compared to vehicle treated controls. (** P value = 0.006, Unpaired t-test, n = 8 per group). **(C)** Average body weight of mice treated with DK1-04e (n = 8) or control vehicle (n = 8) for 6 weeks. **(D)** Immunoblots of global lysine succinylation

and subcellular marker controls (Lamin A/C, Tubulin, Tom20) on mitochondria-enriched fractions of mammary tumor lysates from MMTV-PyMT mice treated with 50mg/kg DK1-04e or vehicle for 6 weeks. Coomassie blue staining was used as a loading control. **(E)** Tumor volume over time in NSG mice engrafted with MDA-MB-231 cells and treated daily with either DK1-04e or vehicle control for 21 days. (*** P value = 0.00014, Linear-Mixed Model, n = 7 tumors per group). **(F)** Representative images of tumors from MDA-MB-231 xenograft mice treated daily with 50mg/kg DK1-04e or vehicle control for 21 days. n = 7 tumors per group. **(G)** Quantification of tumor weight. Xenograft mice treated with DK1-04e had a reduction in tumor size and weight when compared to vehicle controls. (** P value = 0.0079, Unpaired t-test, n = 7 tumors per group). **(H)** Average body weight of mice treated with DK1-04e or control vehicle for 6 weeks. n = 4 mice per group. Data shown in panels B, C, E, G and H are mean values ± standard deviation.